

Oscillatory dynamics of a charged microbubble under ultrasound

Thotreithem Hongray¹, B. Ashok², and J. Balakrishnan^{1,3*}

¹*School of Physics, University of Hyderabad, Central Univ. PO, Gachhi Bowli, Hyderabad 500046, India.*

²*International Institute of Information Technology, Bangalore (I.I.I.T.-B),
26/C, Electronics City, Hosur Road, Bangalore 560100, India. and*

³*School of Natural Sciences & Engineering, National Institute of Advanced Studies (N.I.A.S.),
Indian Institute of Science Campus, Bangalore 560012, India.*

Nonlinear oscillations of a bubble carrying a constant charge and suspended in a fluid, undergoing periodic forcing due to incident ultrasound are studied. The system exhibits period-doubling route to chaos and the presence of charge has the effect of advancing these bifurcations. The minimum magnitude of the charge Q_{min} above which the bubble's radial oscillations can occur above a certain velocity c_1 is found to be related by a simple power law to the driving frequency ω of the acoustic wave. We find the existence of a critical frequency ω_H above which uncharged bubbles necessarily have to oscillate at velocities below c_1 . We further find that this critical frequency crucially depends upon the amplitude P_s of the driving acoustic pressure wave. The temperature of the gas within the bubble is calculated. A critical value P_{tr} of P_s equalling the upper transient threshold pressure demarcates two distinct regions of ω dependence of the maximal radial bubble velocity v_{max} and maximal internal temperature T_{max} . Above this pressure, T_{max} and v_{max} decrease with increasing ω while below P_{tr} , they increase with ω . The dynamical effects of the charge and of the driving pressure and frequency of ultrasound on the bubble are discussed.

PACS numbers: 05.45.-a, 05.90.+m, 43.25.Yw, 43.35.Hl

I. INTRODUCTION

The stability and oscillations of a gas bubble suspended in a liquid under the influence of an acoustic driving pressure field in the ultrasonic frequency range have been the subject of a large volume of scientific literature [1–14]. Studies on the system have been made from different viewpoints coming from its diverse applications and occurrences. Ultrasound is routinely used in medical ultrasonography including echocardiography, lithotripsy, phacoemulsification, use in treatment of cancer and for dental cleansing. Other significant applications of ultrasonic forcing of fluids in which studies of bubble dynamics and

cavitation become very important are in sonochemistry, sonoluminescence, ultrasonic cleaning of materials, waste water treatment and in focussed energy weapons. Cavitation events which involve violent collapse of micron-sized bubbles in the fluid can cause immense damage to the surfaces they are in contact with. Studies of cavitation events in pumps, turbines, surfaces exposed to hydrodynamic flow, etc., continue to be of immense interest in industries and in technological designs of devices.

Rayleigh's study of bubble cavitation was motivated by the need to understand and explain the damage to ships' propellers [1]. Under ultrasonic forcing, the behaviour of a bubble in a fluid depends heavily upon its ambient radius and the amplitude and frequency of the driving sound field. Thus the bubble can show regular oscillatory behaviour which can be periodic or it

*Author to whom correspondence should be addressed. Electronic mail: janaki05@gmail.com

can show highly irregular oscillations which are chaotic and of unpredictable amplitude. For applications where damage caused on surfaces due to bubble cavitation can be disastrous, such as in medicine, it is desirous to operate the sonic device in a “safe” regime, and / or to be able to have control over the bubble’s motion. Often in biological systems, it is known that bubbles in fluids can be electrostatically charged. Studies of the dynamics governing the oscillations, growth and collapse of charged bubbles are therefore of immense relevance because of their prevalence in diverse applications and situations. Experimental and theoretical work on the presence of charge on gas bubbles in fluids goes back to, for example, the work of McTaggart, Alty and Akulichev [9, 10, 16, 17], and more recently the work of Shiran and Watmough and Atchley [11, 12, 18]. None of the work, though, has addressed the issue of dynamics of a charged bubble under ultrasonic forcing.

It is interesting to know what effect the presence of electric charge on the bubble would have and see if the motion of such a charged bubble forced by ultrasound would vary significantly from that of an electrically neutral bubble in a fluid. This especially becomes of practical significance when we are looking at cavitation phenomena in fluids in real-life, be it in the context of cavitation in mechanical systems or in the case of bubbles in fluids in living tissue in a medical context. Apart from the work in [15], we are not aware of any other studies in the literature of the dynamics of acoustically forced charged bubbles suspended in a fluid. Their work however used the value $4/3$ for the polytropic constant which entailed cancellation of all the charged terms; thus their work does not really address the issue of charge which it sets out to do. The extremely nonlinear nature of the system, and the presence of a large number of parameters do not facilitate a straightforward analysis and it becomes essential to take the aid of numerical methods to get an understanding of the dynamics governing the observed behaviour. In this work we

report some studies on the dynamics of a charged bubble in a liquid (which we take to be water) when ultrasound is incident on it. We assume that heat transfer across the bubble takes place adiabatically, and the gas is a monatomic ideal gas. We therefore take the polytropic constant $\Gamma = 5/3$.

In Section II we discuss briefly the nature of the radial dynamics of a charged bubble. Starting with a modified Rayleigh-Plesset equation, we obtain the time series of the bubble radius as also of its radial velocity and temperature. We also calculate the phase portrait of the bubble, under different pressure regimes.

In Section III we discuss the pressure thresholds that influence bubble dynamics; we introduce the expansion-contraction ratio ζ which we had introduced in [23] that enables us to locate the presence of the Blake and upper transient threshold pressures easily when plotted as a function of the driving pressure amplitude P_s . The effects of driving frequency ω and charge on ζ are demonstrated in the present work.

The influence of P_s and ω on the bubble dynamics are investigated in detail in Section IV. We obtain an expression for the minimum charge required on a bubble for radial oscillations to occur at some velocity c_1 , as also the dependence on the forcing pressure amplitude P_s of the maximum forcing frequency ω_H at which an uncharged bubble will oscillate with velocity c_1 .

We then obtain, in Section V, the bifurcation diagrams for the system with driving frequency as the control parameter, and also the bifurcation diagram with charge as the control parameter. We observe that the presence of charge on the bubble advances period-doubling bifurcations with driving frequency as control parameter. Increasing P_s causes the advancement of period doubling and halving bifurcations for charged as well as uncharged bubbles, and bands of chaotic behavior are observed at large P_s .

The effect of charge and driving frequency on the max-

imal temperature are discussed in Section VI. We note that the pressure regime in which the bubble is being forced (whether P_s is above or below the upper transient threshold pressure) determines the frequency dependence of the temperature, and we obtain rough limits on the maximum charge a bubble may carry depending on its ambient radius.

We conclude the paper with a summary of the results in Section VII.

II. RADIAL DYNAMICS OF THE CHARGED BUBBLE

In real-life situations, bubbles in fluids often have some electric charge sticking to them. This has been seen in the case of gas bubbles in various liquids as well as for cavitation events in water. In our work, we adapt the procedures for describing cavitation and forced bubble oscillations (that has a long and extensive literature), to include the presence of charge.

Description of ultrasonically forced bubble motion in a fluid has been made through the Rayleigh-Plesset equation [1–3] and its variants [5, 6, 8, 13, 14, 19–22] modified to take into account compressibility of the fluid or various other factors. Proceeding as we did in our earlier work [23], we further modify the form of the Rayleigh-Plesset equation for the evolution in time of the bubble radius $R(t)$ employed by [19] to include the presence of a constant charge Q on the bubble as follows [15]:

$$\begin{aligned} & \left(\left(1 - \frac{\dot{R}}{c} \right) R + \frac{4\eta}{c\rho} \right) \ddot{R} = \frac{1}{\rho} \left(P_0 - P_v + \frac{2\sigma}{R_0} - \frac{Q^2}{8\pi\epsilon R_0^4} \right) \\ & \times \left(\frac{R_0}{R} \right)^{3\Gamma} \left(1 + \frac{\dot{R}}{c} (1 - 3\Gamma) \right) - \frac{\dot{R}^2}{2} \left(3 - \frac{\dot{R}}{c} \right) \\ & + \frac{Q^2}{8\pi\rho\epsilon R^4} \left(1 - \frac{3\dot{R}}{c} \right) - \frac{2\sigma}{\rho R} - \frac{4\eta}{\rho} \left(\frac{\dot{R}}{R} \right) \\ & - \frac{1}{\rho} (P_0 - P_v + P_s \sin(\omega t)) \left(1 + \frac{\dot{R}}{c} \right) - \frac{R}{\rho c} P_s \omega \cos(\omega t) \quad (1) \end{aligned}$$

R_0 denotes the ambient equilibrium radius of the bubble, P_0 the static pressure, and $P_v = 2.34\text{kPa}$,

the vapour pressure of the gas. We denote by P_s and $\omega = 2\pi\nu$ respectively (ν being the driving frequency), the amplitude and angular frequency of the ultrasound forcing field. We consider water to be the liquid surrounding the bubble, and having density $\rho = 998\text{kg/m}^3$, viscosity $\eta = 10^{-3}\text{Ns/m}^2$, surface tension $\sigma = 0.0725\text{N/m}$, and the velocity of sound in the liquid $c = 1500\text{m/s}$, $P_0 = 101\text{kPa}$, Γ is the polytropic index and $\epsilon = 85\epsilon_0$, where ϵ_0 is the vacuum permittivity.

The modified Rayleigh-Plesset equation above can be simplified and rewritten in dimensionless form [23] as

$$\begin{aligned} & \left(1 - \frac{\dot{r}}{c_*} \right) r\ddot{r} + F\ddot{r} + \frac{\dot{r}^2}{2} \left(3 - \frac{\dot{r}}{c_*} \right) \\ & = H(1 - P_{*v} + M) \left(\frac{1}{r} \right)^{3\Gamma} \left(1 + \frac{\dot{r}}{c_*} (1 - 3\Gamma) \right) \\ & + \frac{C}{r^4} \left(1 - \frac{3\dot{r}}{c_*} \right) - S \frac{1}{r} - F c_* \left(\frac{\dot{r}}{r} \right) \\ & - H(1 - P_{*v} + P_{*s} \sin(\tau)) \left(1 + \frac{\dot{r}}{c_*} \right) - H \frac{r P_{*s}}{c_*} \cos(\tau) \quad (2) \end{aligned}$$

where $r = R/R_0$, $\tau = \omega t$, $P_{*v} = P_v/P_0$, $P_{*s} = P_s/P_0$ and the overdot here corresponds to differentiation with respect to τ , and where the following dimensionless constants have been used:

$$\begin{aligned} c_* &= \frac{c}{R_0\omega}; \quad F = \frac{4\eta}{\rho R_0 c}; \quad H = \frac{P_0}{R_0^2 \omega^2 \rho}; \\ M &= \frac{1}{P_0} \left(\frac{2\sigma}{R_0} - \frac{Q^2}{8\pi\epsilon R_0^4} \right) \\ C &= \frac{Q^2}{8\pi\epsilon R_0^6 \omega^2 \rho}; \quad S = \frac{2\sigma}{\rho R_0^3 \omega^2} \end{aligned}$$

We have employed the dimensionless form of the equations for obtaining their numerical solutions. In all the expressions that follow, and in the numerical results shown in graphs, we have rescaled the quantities by the appropriate factors and only displayed the dimensional form for a physical grasp of the magnitudes of the quantities involved.

The presence of charge Q counters the effect of surface tension, reducing its effective value, and induces several

interesting changes to the dynamics of bubble oscillations. In a previous work [23] we had obtained for the charged bubble, the Blake threshold and radius and also some results for the upper transient threshold for cavitation. In the following sections, we describe some interesting consequences of the presence of charge on a bubble.

As the bubble expands and contracts, the surface charge density decreases or increases respectively. The presence of charge lowers the surface tension and for sub-micron sized bubbles, dominates over it, influencing the minimum and maximum values of the radius and the maximum velocities achieved by the bubble, and changing its point of collapse. A charged bubble achieves higher temperatures within it than an uncharged one, the collapse of the bubble being more violent in the charged case.

The above results indicate that since the bubble oscillations are more energetic for the charged bubble, the temperature attained by the gas within the bubble during its oscillations, would be higher as well. To confirm this, we calculate the temperature using equation (3) [20].

$$T(t) = T(0) \left(\frac{R_0^3 - h^3}{R^3 - h^3} \right)^{\Gamma-1}, \quad (3)$$

where h is the van der Waals hard core radius for the gas, $h = R_0/8.86$ for Argon [22]. This equation is obtained under the assumption that there is no exchange of heat from the gas to its surroundings, that the system is essentially adiabatic.

This assumption is not strictly true as in reality the equation of state of the gas enclosed within the bubble can be either adiabatic or isothermal, depending upon the rate of collapse of the bubble and whether or not the various relaxation time-scales permit thermal diffusion to occur to and from the bubble. We use the expression in order to get an idea of the magnitudes achievable by the temperature in the presence of charge. To better visual-

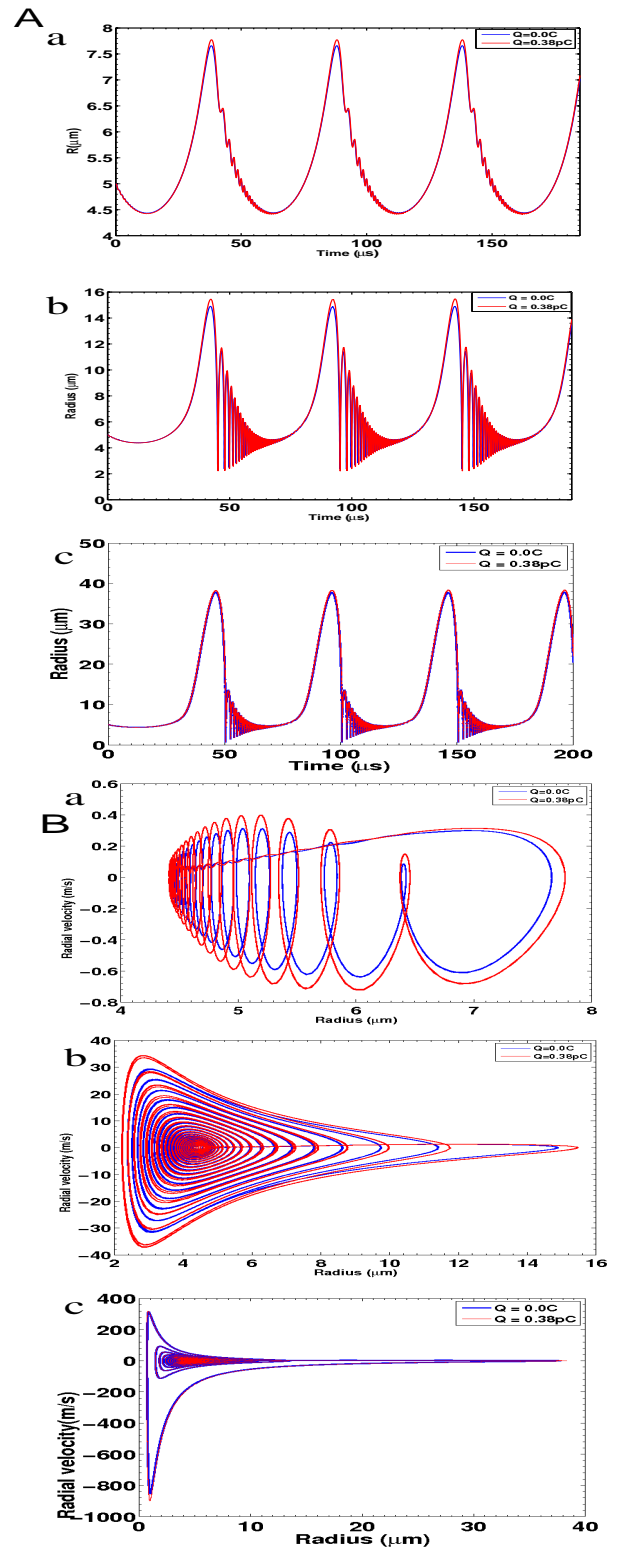


FIG. 1: A. Time series of R , and B. Phase portrait (R vs \dot{R}), for $R_0 = 5\mu\text{m}$ and bearing charge $Q = 0$ (blue online) and $Q = 0.38\text{pC}$ (red online), $P_s =$ (a) $1.0P_0$, (b) $1.12P_0$, (c) $1.25P_0$. Amplitudes of R , \dot{R} are larger; the phase portrait spans a larger space for the charged bubble than for the uncharged case (color online).

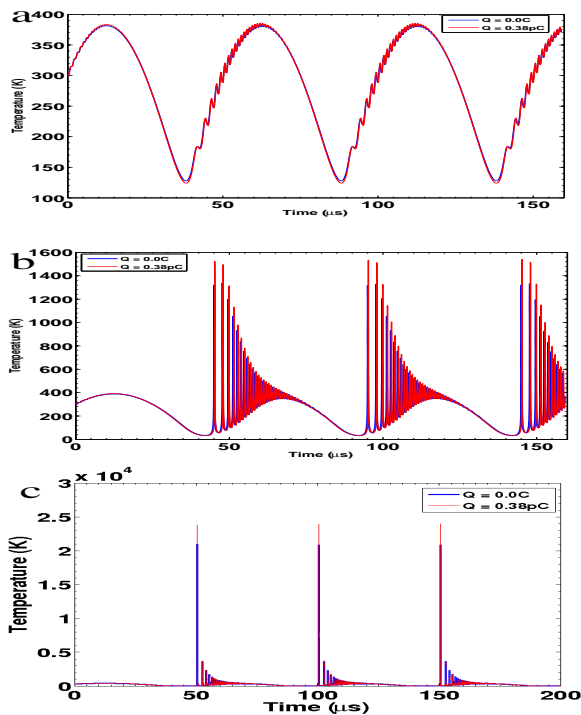


FIG. 2: Time series of temperature (in K) plotted as a function of time for $R_0 = 5\mu m$ at driving frequency $\nu = 20kHz$, and bearing charge $Q = 0$ (blue online) and $Q = 0.38pC$ (red online) for three values of P_s : (a) $1.0P_0$, (b) $1.12P_0$, (c) $1.25P_0$. Temperatures T are larger for the charged bubble than for the uncharged case (color online).

ize the effect that the amplitude of the forcing pressure P_s and charge Q have on the bubble dynamics, we consider a bubble being driven at 20 kHz, i.e., the lower limit of the ultrasonic spectrum. Even in this lowest ultrasonic regime, the time series of bubble radius, radial velocity, and temperature all show an enhancement in values due to charge. Moreover, P_s crucially determines the dynamics of the bubble as illustrated in Figures (1,2 A-B, a,b,c). We have considered three values of P_s , $P_s = 1.0P_0$, $1.12P_0$ and $1.25P_0$. These pressures are, respectively, below the Blake threshold P_{Blake} , at the upper transient pressure threshold P_{tr} , and above P_{tr} . As can be seen, the pressure regime in which the bubble dynamics occurs, crucially determines the behavior. At $P_s = 1.0P_0$, $T_{max} \approx 370K$, the uncharged bubble temperature being marginally less than that for the charged

bubble ($Q = 0.38 pC$); for $P_s = P_{tr} = 1.12P_0$, T_{max} goes up to about 1520 K for the charged bubble and about 1320 K for the uncharged case; and for $P_s = 1.25P_0$, T_{max} shoots up still further, to about 24,000 K for the charged (and approximately 21,000 K for the uncharged) bubble. These temperatures vary by orders of magnitude and spell out the importance of P_s and Q .

III. PRESSURE THRESHOLDS

The Blake threshold determines the pressure threshold beyond which an acoustically forced bubble undergoes drastic expansion. After the Blake threshold and preceding the onset of bubble collapse following a larger threshold known as the upper transient threshold, P_{tr} , the bubble is essentially in an unstable regime.

Depending upon whether the amplitude of the applied acoustic forcing pressure is greater or lesser than P_{tr} , the response of the bubble to the frequency of the applied pressure wave varies drastically.

At low amplitudes of the forcing pressure (i.e., $P_s < P_{tr}$), increasing driving frequency causes a proportional increase in the bubble's maximum radial velocity v_{max} . This happens upto some critical value of the frequency for that P_s after which v_{max} rises more steeply but accompanied with large oscillations.

At larger amplitudes of the forcing pressure, with P_s approaching the value of the Blake and upper transient threshold pressures, the situation is different. v_{max} first decreases with increasing driving frequency upto a frequency ω_{hc} , after which v_{max} rises with frequency but with large oscillations. As could be expected from the above observations, a similar observation can be made regarding the maximum temperature T_{max} of the gas inside the bubble.

A useful graphical illustration of the transient threshold pressures, i.e. of the Blake threshold (P_{Blake}) and the upper transient threshold (P_{tr}) pressures, can be obtained

by plotting $\zeta = (R_{max} - R_0)/(R_0 - R_{min})$ as a function of the amplitude of driving pressure. This quantity

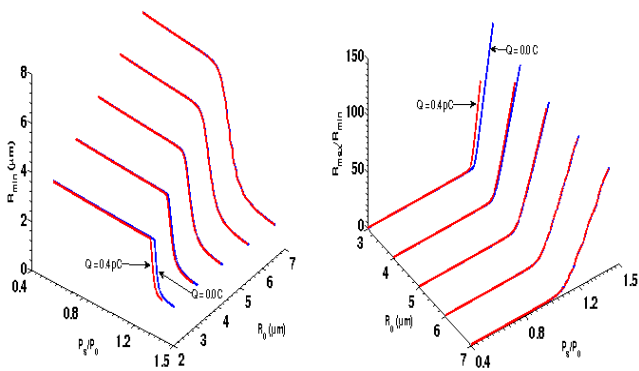


FIG. 3: Plots of R_{min} (left) and R_{max}/R_{min} (right) as functions of P_s for different values of ambient radius (for $Q = 0$ and $Q = 0.4$ pC) at 20kHz forcing frequency. (color online).

ζ , which we call the expansion-contraction ratio, handily shows the location of both the Blake and the upper transient thresholds. Both these thresholds cannot be identified easily at the same time from, for example, a plot of R_{max}/R_{min} as a function of applied pressure amplitude. In Figure (3), the points of inflection of the curves correspond to the Blake threshold pressures for the respective R_0 values. The effect of charge is clearly seen in reducing the threshold pressure as compared to the charged case. The upper transient threshold cannot be easily pinned down from this plot. While the Blake threshold is indicative of the threshold of the expansive growth of the bubble, the upper transient threshold demarcates where the violent collapse of the bubble occurs. A plot of ζ versus P_s for different values of R_0 as shown in Figure (4) shows a rise of the curve till it peaks (at $P_s = P_{Blake}$) followed by a trough or well (at $P_s = P_{tr}$) before rising up steeply for higher P_s (this has been discussed in some detail in our earlier work [23]). At pressures between P_{Blake} and P_{tr} the bubble is in an unstable regime. This also explains the presence of large fluctuations or oscillations in the velocity vs. frequency plots at such intermediate pressures. The presence of charge shifts the threshold pressures to lower values. With increasing ambient ra-

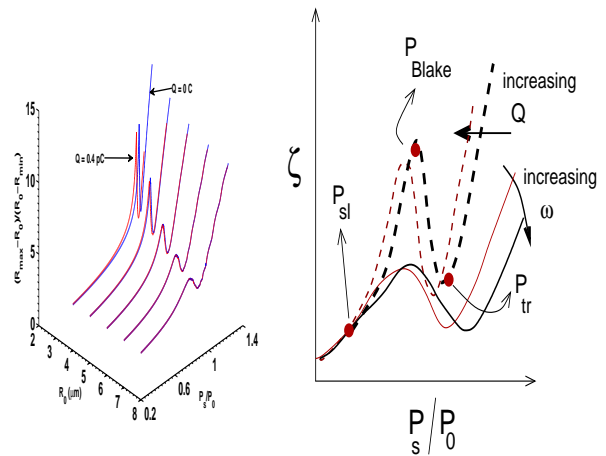


FIG. 4: Plot of $\zeta = (R_{max} - R_0)/(R_0 - R_{min})$ as a function of forcing pressure amplitude P_s and R_0 at 20kHz. The schematic at right shows the locations of the Blake threshold pressure and the upper transient threshold pressure on the $\zeta - P_s$ curve. Increasing bubble charge shifts the curve down and to the left, while increasing driving frequency decreases the steepness of the curve and flattens it.(color online).

dius R_0 , ζ loses its distinctive peak-valley appearance gradually.

The maximum radius attainable by the bubble gradually increases with charge for a given driving frequency [23]. This can be understood from the fact that the presence of charge on the bubble decreases the effective surface tension. This causes the bubble to expand more easily in the negative pressure field. A casual reading might give rise to the observation that by the same argument, the minimum radius reached by the bubble would likewise follow a similar trend, with R_{min} for a charged bubble having a larger value than that of a neutral bubble. However, this is not so. It should be borne in mind that R_{min} is influenced by the maximal velocity the bubble is able to reach. The greater the velocity, the smaller the R_{min} that it collapses to. Hence, perhaps counter-intuitively, charged bubbles undergoing forced oscillations, will achieve smaller values of R_{min} than electrically neutral bubbles.

Thus presence of charge leading to greater bubble expansion, in turn results in the bubble collapse being much

more rapid and violent, shrinking the bubble volume more than in the case of the uncharged bubble. This can be seen in Figure (3) (left), where the minimum radius, R_{min} , reached by the bubble at the moment of collapse is plotted as a function of the driving pressure P_s and R_0 for the charged and uncharged bubble. As was shown in greater detail in our earlier work [23], R_{min} reduces with increasing Q .

IV. INFLUENCE OF AMPLITUDE AND FREQUENCY OF DRIVING PRESSURE FIELD

The maximum radial velocity of the bubble attained during its collapse or contracting phase depends also on the driving frequency, the charge present on the bubble, as well as the amplitude of the driving pressure wave, as also on the initial radius R_0 of the bubble in its quiescent state. Figure 5 are plots of the maximal radial velocity as functions of the driving frequency (a) and pressure P_s (b). There are several interesting features evident from the figures.

The behaviour of v_{max} above $P_s = P_{tr}$ is different from that below it. The plots shown are for a bubble of $R_0 = 5\mu m$ for which $P_{tr} = 1.12P_0$. Fig.(5a) shows that at $P_s < P_{tr}$, v_{max} increases as a function of driving frequency ν while for $P_s > P_{tr}$ Fig.(5b), it decreases. Increasing the driving frequency induces instability by producing large amplitude oscillations.

For a given magnitude of pressure amplitude P_s , the magnitude of charge present influences the dynamical regime of the bubble. If the driving angular frequency of the applied pressure wave is ω at a certain pressure amplitude, for bubble oscillations to occur with some maximal radial velocity $\dot{R} = c_1$, the charge present on the bubble should have some minimum magnitude $Q = Q_{min}(\omega)$. At low frequencies, even an uncharged bubble might oscillate at that velocity; however at higher frequencies, if charge $Q < Q_{min}$, the radial bubble velocity would be smaller than c_1 . This is because as frequency increases,

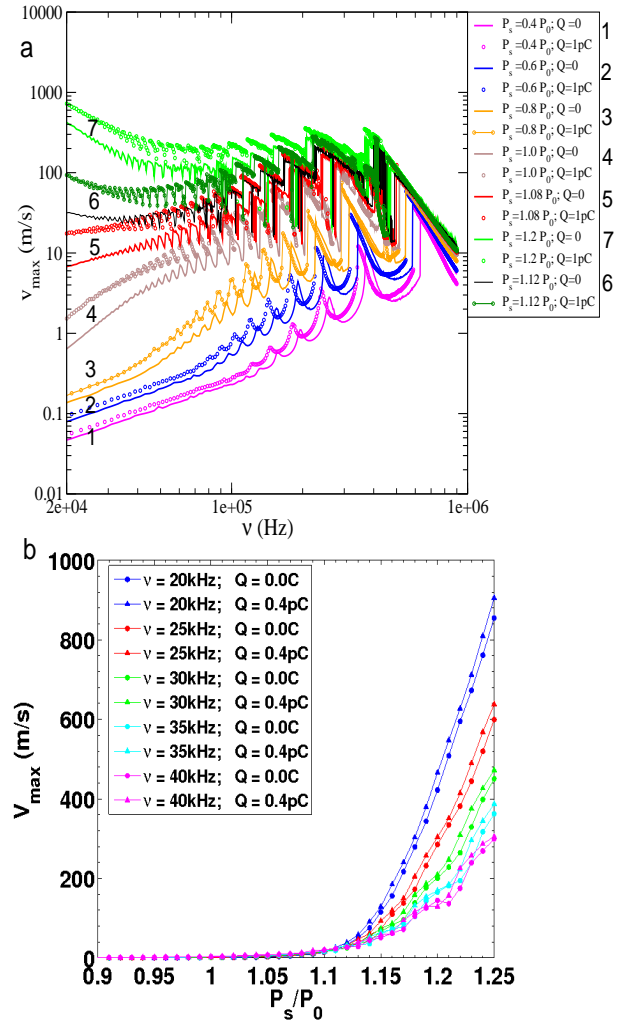


FIG. 5: Maximum velocity vs (a) driving frequency, plotted at 7 different P_s values and for zero & non-zero values of charge; the $P_s = 1.12P_0$ curves (number 6, darkest ($Q = 0$ black online) & just above that ($Q = 1pC$, dark green online)) correspond to the upper transient threshold pressure P_{tr} (for $R_0 = 5\mu m$) and clearly demarcate distinct behaviour for $P_s > P_{tr}$ and $P_s < P_{tr}$. (b) v_{max} vs. P_s for different frequencies (20 to 40 kHz, increasing from left to right), for zero (\bullet) and non-zero ($Q = 0.4pC$, triangle) charge. (color online).

the bubble does not get sufficient time to complete its expansion, so that its subsequent collapse occurs with smaller radial velocity than if expansion to a greater size had been done. The presence of charge reduces the surface tension and encourages expansion to larger radial

dimension and the consecutive, more violent collapse to a smaller radius.

That the change in $Q_{min}(\omega)$ with ω show a bifurcation in the parameter space is clear from Figure 6. This transition from zero to non-zero Q_{min} occurs at an angular frequency ω_H . For $P_s = 1.35P_0$ and $R_0 = 5\mu\text{m}$, $\omega_H = 23\text{kHz}$. The magnitude of Q_{min} varies with driv-

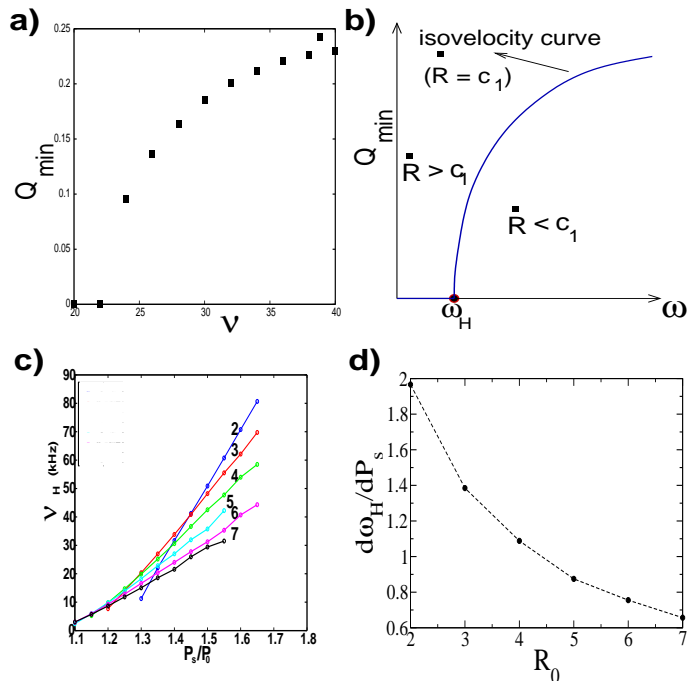


FIG. 6: Q_{min} versus frequency ω iso-velocity plots ($v \approx 1500$ m/s) for a) $R_0 = 5\mu\text{m}$, for $P_s = 1.35P_0$ (Q_{min} is in pC, ω in kHz); b) schematic illustrating the nature of the iso-velocity plot, $Q_{min} \sim (\omega - \omega_H)^{0.25}$; c) plot showing the dependence of ω_H on P_s for different values of R_0 (curves 2,3,4,5,6,& 7 correspond to corresponding R_0 values in μm); d) plot illustrating variation of $(d\omega_H/dP_s)$ with R_0 . (color online).

ing frequency as

$$Q_{min} \approx a(\omega - \omega_H)^b, \quad (4)$$

where the prefactor a has appropriate dimensions and depends on the value of the initial ambient bubble radius R_0 , and $b \approx 0.25$.

We could attempt to give a simple explanation for the frequency dependence of Q_{min} . We could argue that for a given value of constant maximal radial velocity c_1 , the

kinetic energy of the bubble would scale as the electrostatic contribution $\sim Q^2/R_{min}$, so that $Q^2 \sim a_2 c_1 R_{min}$, a_2 being a prefactor with appropriate dimensions. Since for high applied pressures (that is, for values of P_s above the Blake threshold pressure or of the order of or above the upper transient threshold pressure) we know that the minimum bubble radius scales as the two-fifths power of the driving frequency $R_{min} \propto \omega^{2/5}$, it would follow that $Q^2 \propto c_1 \omega^{2/5}$ so that $Q \propto \omega^{0.2}$, which is close but not equal to the observed exponent of 0.25. Hence, this argument, while it serves to give a lower bound for Q_{min} , is insufficient.

Proceeding more systematically therefore, we start by making a linearization of the Rayleigh-Plesset equation. Proceeding along the lines of [5], the driving sound pressure is introduced through a small perturbation α , so that the total external field P_{ext} can be written as:

$$P_{ext} = P_0(1 - \alpha \cos \omega t) \quad (5)$$

The bubble oscillations $R(t)$ about the equilibrium radius R_0 can then be expressed as

$$R = R_0(1 + x(t)) \quad (6)$$

where $x(t)$ is a small quantity of order α . Substituting this equation in the Rayleigh-Plesset equation (1) and linearizing it, we get

$$\ddot{x} + \beta \dot{x} + \omega_0^2 x = -F_{ext} \quad (7)$$

where the damping coefficient β , natural frequency of oscillation ω_0 of the bubble and F_{ext} are given by

$$\beta = \frac{1}{\rho c R_0 \left(1 + \frac{4\eta}{c\rho R_0}\right)} \left(4\phi/R_0^5 + \frac{3Q^2}{8\pi\epsilon R_0^4} + \frac{4\eta c}{R_0}\right)$$

$$\omega_0^2 = \frac{1}{\rho R_0^2 \left(1 + \frac{4\eta}{c\rho R_0}\right)} \left(5\phi/R_0^5 - \frac{2\sigma}{R_0} + \frac{4Q^2}{8\pi\epsilon R_0^4}\right) \quad (8)$$

Here only terms linear in x and its derivatives have been retained and ϕ/R_0^5 is the equilibrium gas pressure in the bubble defined by

$$\phi/R_0^5 = (P_0 - P_v + \frac{2\sigma}{R_0} - \frac{Q^2}{8\pi\epsilon R_0^4}). \quad (9)$$

The particular situation of looking for conditions where the radial velocity is constant is thus implicitly satisfied. In eqn.(7), F_{ext} is given by

$$F_{ext} = -P_s \frac{\left(1 + \frac{R_0^2 \omega^2}{c^2}\right)^{\frac{1}{2}}}{\left(R_0^2 + \frac{4\eta R_0}{c\rho}\right)} \times \cos\left(\omega t - \arctan\left(\frac{c}{R_0 \omega}\right)\right) \\ \approx -P_s \frac{\left(1 + \frac{R_0^2 \omega^2}{c^2}\right)^{\frac{1}{2}}}{\left(R_0^2 + \frac{4\eta R_0}{c\rho}\right)} \cos\left(\omega t - \frac{\pi}{2} + \frac{R_0 \omega}{c}\right) \quad (10)$$

where in arriving at the last line of eqn.(10), use has been made of the fact that $\frac{R_0 \omega}{c} \ll 1$. Scaling the time as $\hat{t} = \omega_0 t$ for convenience, eqn.(7) can be solved exactly. Dropping the hat ($\hat{\cdot}$) over t for convenience of notation in all of the following, the steady state part of the solution is found to be

$$x = -\frac{P_s \left(1 + \frac{R_0^2 \omega^2}{c^2}\right)^{\frac{1}{2}}}{\rho \left(R_0^2 + \frac{4\eta R_0}{c\rho}\right)} \frac{1}{(\omega_0^2 - \omega^2)^2 + \omega^2 \beta^2} \\ \times \left((\omega_0^2 - \omega^2) \cos\left(\frac{\omega}{\omega_0} t + \theta\right) + \omega \beta \sin\left(\frac{\omega}{\omega_0} t + \theta\right) \right) \quad (11) \\ v = \dot{x} = -\frac{P_s \left(1 + \frac{R_0^2 \omega^2}{c^2}\right)^{\frac{1}{2}}}{\rho \left(R_0^2 + \frac{4\eta R_0}{c\rho}\right)} \frac{\omega}{\omega_0} j a \frac{1}{(\omega_0^2 - \omega^2)^2 + \omega^2 \beta^2} \\ \times \left(-(\omega_0^2 - \omega^2) \sin\left(\frac{\omega}{\omega_0} t + \theta\right) + \omega \beta \cos\left(\frac{\omega}{\omega_0} t + \theta\right) \right) \quad (12)$$

where θ denotes the phase.

Combining eqns.(11) and (12) we obtain

$$\frac{\omega^2}{\omega_0^2} x^2 + v^2 = \frac{\omega^2}{\omega_0^2} \frac{P_s^2}{R_0^4 \rho^2 \left(1 + \frac{4\eta}{c\rho R_0}\right)^2} \frac{1}{\left((\omega_0^2 - \omega^2)^2 + \omega^2 \beta^2\right)} \quad (13)$$

Again using eqn.(6) to rewrite $x = R/R_0 - 1$, and $v = \dot{R}/R_0$ in eqn.(13), we obtain after some algebra an equation for ω :

$$\omega^4 + \frac{K}{\rho^2 R_0^4 \left(1 + \frac{4\eta}{c\rho R_0}\right)^2} \omega^2 + \frac{G^2}{\rho^2 R_0^4 \left(1 + \frac{4\eta}{c\rho R_0}\right)^2} = 0 \quad (14)$$

where

$$G = 5(P_0 - P_v) + \frac{8\sigma}{R_0} - \frac{Q^2}{8\pi\epsilon R_0^4} \\ K = -\frac{2R_0^2}{c^2} (c^2 \rho + P_0 - P_v) G + \frac{R_0^2}{c^2} \left(\frac{4\eta c}{R_0} - (P_0 - P_v)\right)^2 \\ - \frac{R_0^6 P_s^2 \rho \left(1 + \frac{4\eta}{c\rho R_0}\right)}{\left[\rho R_0^4 \left(1 + \frac{4\eta}{c\rho R_0}\right) (R^2 - 2RR_0 + R_0^2) + G\dot{R}^2\right]} \quad (15)$$

This leads to the following expression for ω

$$\omega = \frac{1}{\rho R_0^2 \left(1 + \frac{4\eta}{c\rho R_0}\right)} \\ \times \left[-K \pm \left(K^2 - 4\rho^2 R_0^4 \left(1 + \frac{4\eta}{c\rho R_0}\right)^2 G^2 \right)^{1/2} \right]^{1/2} \quad (16)$$

After a careful look at each of the terms in this equation, we find that the dominant contribution of Q to $d\omega/dQ$ occurs as a cubic term :

$$\frac{d\omega}{dQ} \sim a_3 Q^3, \quad (17)$$

a_3 being a prefactor with appropriate dimensions. Integrating both sides of this equation between the limits corresponding to $Q = 0$ and Q gives

$$\omega - \omega_H \sim a_3 Q^4, \quad (18)$$

where ω_H is the frequency for the bubble with zero charge at which the $\dot{R}_{max} = c_1$, so that

$$Q \sim a'_3 (\omega - \omega_H)^{1/4}, \quad (19)$$

(the prefactor a'_3 having appropriate dimensions), reproducing eqn.(4) that was obtained from an analysis of the numerical results shown in the plots in Figure (6). Hence it is very easy to predict the minimum charge Q_{min} required on a bubble at a given applied pressure amplitude for attaining some particular value of the bubble's radial velocity, once ω_H is known.

There is another interesting feature to be noted in this transition. The value of the frequency ω_H depends on the magnitude of the amplitude P_s of the driving pressure wave. Indeed, for a given ambient bubble radius R_0 , ω_H takes the simple linear form

$$\omega_H = b_1 + b_2 P_s, \quad (20)$$

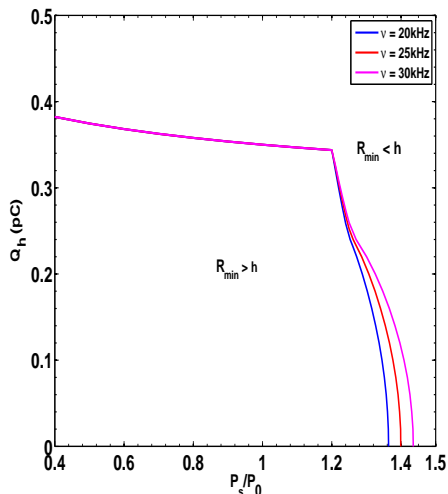


FIG. 7: Q_h as function of P_s for a bubble of $R_0 = 2\mu m$ for three different values of driving frequencies ν . The value of P_s at which $Q_h = 0$, increases with increasing frequency. The physically reachable region is the area below the curve corresponding to $R_{min} > h$. The region above the curve corresponds to the (unphysical) regime where $R_{min} < h$. (color online).

where b_1 and b_2 vary with R_0 . This can be seen clearly from the plot (Figure (6)c). A further functional dependence of b_2 on R_0 , that is, of the slope $d\omega_H/dP_s$ on R_0 , is also found (Figure (6)d), and is of the form

$$\frac{d\omega_H}{dP_s} \sim R_0^{-0.9}. \quad (21)$$

The maximal charge, Q_{max} , which a bubble can carry, is bounded by the fact that beyond a value Q_h of the charge, bubble dimensions may reduce to below the value of the van der Waals hard core radius for the gas enclosed, which is physically untenable.

Hence, the value of Q_h , the physically feasible maximal limit to the charge the bubble may carry, will be less than Q_{max} for a particular R_0 . Moreover, it depends as well on the amplitude of the forcing pressure P_s , with Q_h decreasing with increasing P_s and also with decreasing driving frequency. Figure (7) show plots of Q_h as a function of P_s for three different driving frequencies, for $R_0 = 2\mu m$. Below a certain value of P_s , Q_h becomes

nearly independent of frequency as well as P_s .

V. BIFURCATION DIAGRAMS

That the driving frequency influences the bubble dynamics is unquestionable. Techniques of dynamical systems theory have been used for long in the literature to understand bubble stability under variation of parameters (see for example [19, 24–27]. Parlitz, et al. [19] have, in their work, extensively investigated the frequency bifurcation diagrams for the bubble radius at various values of the driving amplitude pressure, P_s .

In Figs.(8-11) we have shown the bifurcation diagrams for the maximum radial amplitude R_{max} of the given time series of the bubble, with the driving frequency as the control parameter for $R_0 = 1.45\mu m, 2\mu m$ and $5\mu m$ for uncharged and charged bubbles.

The bifurcation diagrams for various sets of parameters are constructed by sampling the time series after making sure the transients have decayed, for every time period $T = 1/\nu$ of the external acoustic driving pressure elapsed. These sample points are precisely the points of intersection of the trajectories in phase plane with the Poincare cross section, and the orbit formed by the points represents the Poincare map. The bifurcation diagram is then constructed by plotting the sampled points calculated for a range of values of the control parameter (frequency or charge) and then plotting it with the control parameter on the horizontal axis and the sampled points on the vertical axis.

In the response curves where period-doubling bifurcations occur, the branches always merge back to give period-1 oscillations.

The presence of non-zero charge on the bubble advances period-doubling bifurcations with the driving frequency as the control parameter. This is demonstrated in the bifurcation diagrams in Figs.(8-9). For an uncharged bubble with ambient radius R_0 of 2microns at a driving

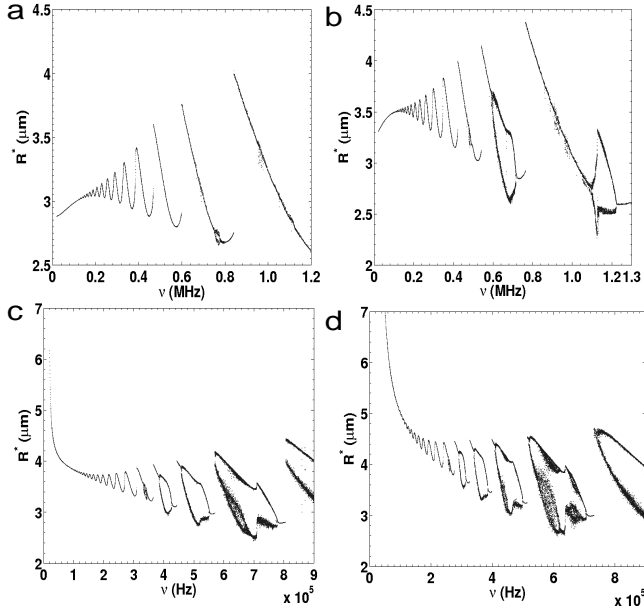


FIG. 8: Bifurcation diagram of a bubble oscillator with driving frequency as the control parameter, and for $R_0 = 2\mu\text{m}$ and (top): $P_s = 1.2P_0$ (i.e., $P_s < P_{tr}$), and (bottom): $P_s = P_{tr} = 1.3P_0$. $Q = 0$ in (a) and (c), and $Q = 0.2pC$ in (b) and (d).

pressure of $1.2P_0$, period doubling is first seen at around 720kHz for the uncharged bubble, while the presence of 0.2pC charge advances it to about 600 kHz (Fig.(8, a,b)). We observe that there are no chaotic regimes present at least till driving frequencies of 1000kHz for low driving pressures such as this.

Figs.(8-10) show that increasing the external pressure P_s also has the effect of advancing the succession of period-doubling-period-halving bifurcations both for the charged as well as for the uncharged systems. For instance at $1.3P_0$ (Figs.8 c,d), the first period doubling bifurcation occurs at a forcing frequency of approximately 320kHz, followed by period halving bifurcation at 350kHz leaving period 1 oscillations, whereas on introduction of charge $Q = 0.2pC$, the first period doubling bifurcation makes its appearance much earlier, at about 295 kHz, only to merge back to period 1 oscillations through a period halving bifurcation at 315 kHz. As one increases the driving frequency further, one observes the occurrence of

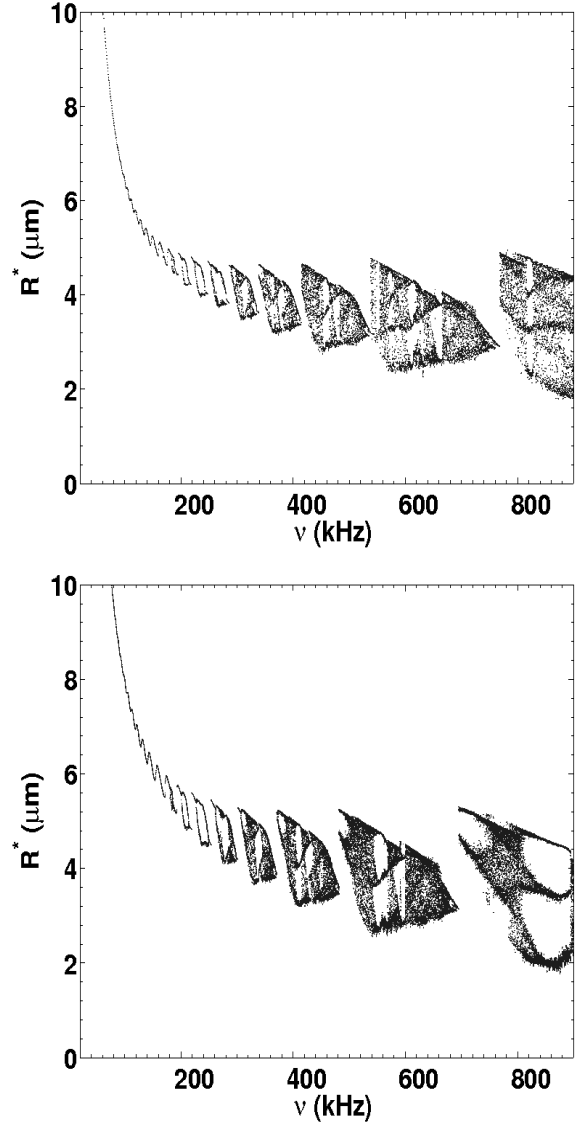


FIG. 9: Bifurcation diagram with respect to driving frequency of a bubble oscillator with $R_0 = 2\mu\text{m}$ and $P_s = 1.4P_0$ for an uncharged bubble (top) and having charge $Q = 0.2pC$ (bottom). (Note that $P_s > P_{tr}$.)

a sequence of period-doubling - period-halving bifurcations.

It should be noted that the chaotic regions make their appearance at the upper transient threshold pressure P_{tr} (which for an uncharged bubble of $R_0 = 2\mu\text{m}$ is $1.3P_0$), and become more prominent for $P_s > P_{tr}$ (Fig.9). At large driving pressures, bands of chaotic regimes are present at high values of the forcing frequency, in agreement with observations of time series data. We

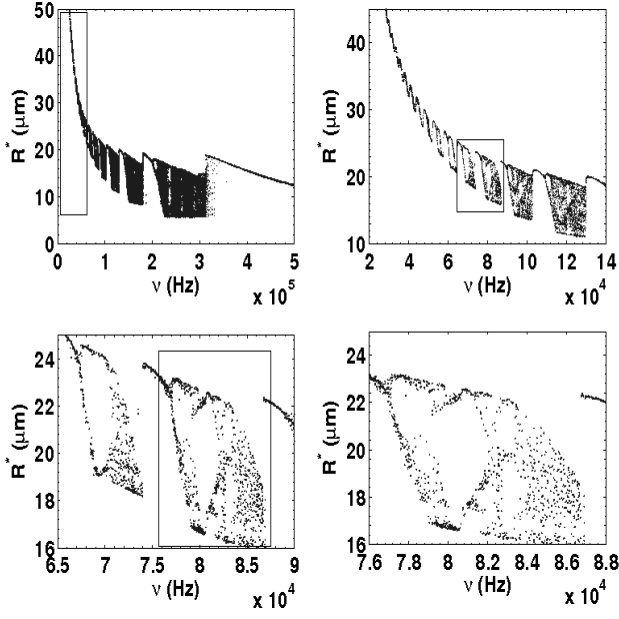


FIG. 10: Bifurcation diagram with respect to driving frequency of a bubble oscillator with $R_0 = 5\mu\text{m}$ and for $Q = 0.8\text{pC}$. The driving pressure $P_s = 1.4P_0$ (Here, $P_s > P_{tr}$). Successive images (b,c,d) show magnification of preceding insets showing period-doubling and chaos.

show this in Figs.(9) for $P_s = 1.4P_0$: chaotic behaviour is seen to be present even at around 270-300kHz for charged and uncharged bubbles.

In Figs.(10) the sequence of period-2 and period-1 oscillations generated is shown for a slightly larger bubble, with $R_0 = 5\mu\text{m}$ and bearing charge $Q = 0.8\text{pC}$, driven at pressure amplitude $P_s = 1.4P_0$.

From these observations and other plots (not shown here) we deduce that the maximal radial amplitude of the bubble of a given equilibrium radius R_0 shows chaotic behaviour as a function of the driving frequency ν , for $P_s \geq P_{tr}$ at large values of ν . It was shown in [23] that $P_{tr} = 1.12P_0$ for $R_0 = 5\mu\text{m}$ and $P_{tr} = 1.3P_0$ for $R_0 = 2\mu\text{m}$ for the uncharged bubble.

For smaller frequencies, such as in the sonoluminescent regime, the presence of charges do not appear to introduce period-doublings in the system. However, the

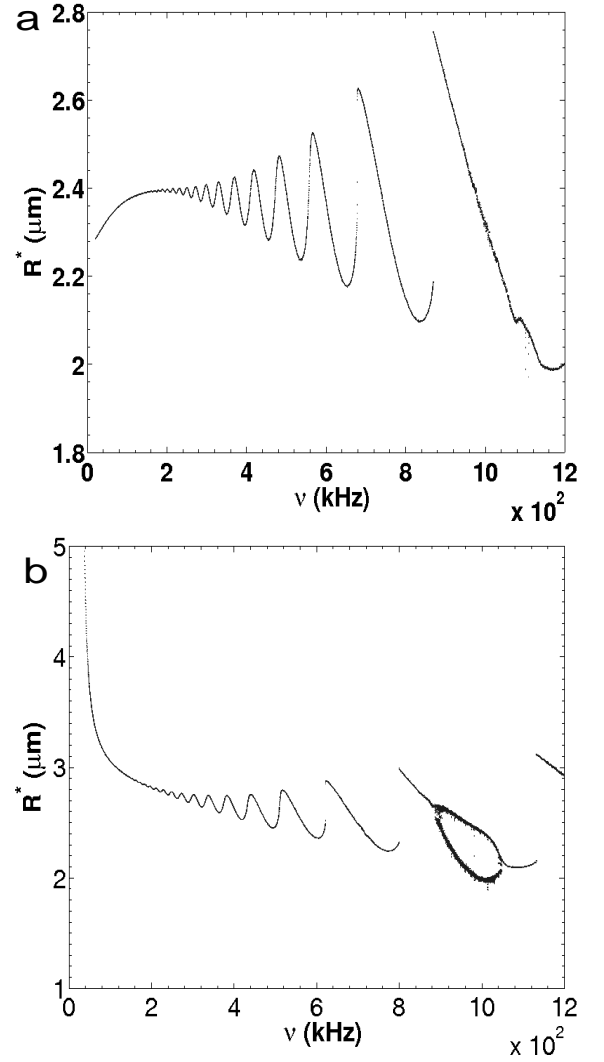


FIG. 11: Bifurcation diagram of a bubble oscillator with driving frequency as the control parameter for a smaller bubble. $R_0 = 1.45\mu\text{m}$ and $P_s = 1.4P_0$. (a) $Q = 0$; (b) $Q = 0.1\text{pC}$.

effect of charges in bringing about drastic changes in the bubble stability is more pronounced for smaller values of R_0 . This is demonstrated in Figs.(11 a,b) for a bubble with $R_0 = 1.45\mu\text{m}$ and driving pressure amplitude P_s of $1.4P_0$.

The presence of 0.1pC charge on the bubble (Figs.(11b)) induces a period-doubling bifurcation at a driving frequency of 880 kHz followed in quick succession by a period-halving bifurcation at 1040 kHz. These are absent for an uncharged bubble (Fig.(11a)).

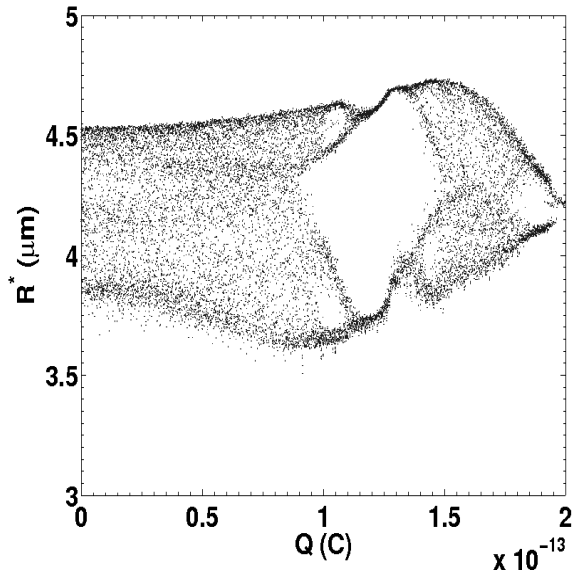


FIG. 12: Bifurcation diagram of a bubble oscillator with charge Q as the control parameter, and with $R_0 = 2\mu\text{m}$ and $P_s = 1.4P_0$ and at $\nu = 300\text{kHz}$. Non-chaotic windows are seen, most prominent one centred around $Q = 0.125pC$.

In Fig.(12) we obtain the bifurcation diagram of a bubble of $R_0 = 2\mu\text{m}$ driven by sonic pressure amplitude of $1.4P_0$ and frequency 300 kHz with charge as the control parameter. The choice of 300 kHz for the driving frequency has been made using the bifurcation diagram with frequency as the parameter (Fig.(9)) where the system is just beginning to get chaotic at this frequency. In Fig.(12) we see an interesting non-chaotic region centered around $Q = 0.125pC$ with period-doubling and period-halving cascades. While constructing the bifurcation diagrams care has been taken to ensure that we work only within the range of charges permissible for a bubble of a given ambient radius.

VI. THE COLLAPSING BUBBLE: FREQUENCY & CHARGE DEPENDENCE OF TEMPERATURE

Investigating the maximum temperature as a function of the driving frequency, we obtain the interesting result that there exist two distinct domains of behavior of

T_{max} depending upon the amplitude of the driving pressure, P_s .

At lower pressures, i.e, for $P_s < P_{tr}$ (for example for $P_s = 1.1P_0$ for $R_0 = 5\mu\text{m}$), T_{max} increases with driving frequency. However, as this value of P_s falls in the vicinity of the transient threshold in the unstable regime (Fig.(4a)), we would expect T_{max} to show large oscillations with frequency, as is also seen in Fig.(13a).

At higher pressures, i.e, for $P_s > P_{tr}$ (for example for $P_s = 1.25P_0$ for $R_0 = 5\mu\text{m}$), the maximal temperature's frequency dependence is the opposite, with T_{max} decreasing uniformly with increasing frequency, showing oscillatory behavior (Fig.(13b)). T_{max} shows a frequency-dependence of the form

$$T_{max} = a_4 \times (\nu - a_5)^{-4/5}, \quad (22)$$

a_4 and a_5 being constants with appropriate dimensions. This is understood by recalling that the temperature is obtained from

$$T = T(0) \left(\frac{R_0^3 - h^3}{R^3 - h^3} \right)^{2/3}, \quad (23)$$

for $\Gamma = 5/3$. Making the approximation that $(h/R_0)^3 < 1$ and also that $(h/R)^3 < 1$ is sufficiently small at most values of R , we can approximate Eqn.(23) by

$$T \approx T(0)R_0^2/R^2. \quad (24)$$

Since at regimes at or near the Rayleigh collapse, $R(t) \sim \omega^{2/5}$, it immediately follows that

$$T(t) \propto \omega^{-4/5}. \quad (25)$$

Values of T_{max} at lower pressures are less than that at higher pressures. Temperature T_{max} rises steeply with pressure P_s after some critical value of the pressure that equals the upper transient pressure threshold. Temperature calculations have also been reported by Wu and Roberts [28] and Yasui [29] giving high magnitudes of the temperature. The presence of charge serves to reduce the pressure at which a maximum temperature T_{max} is

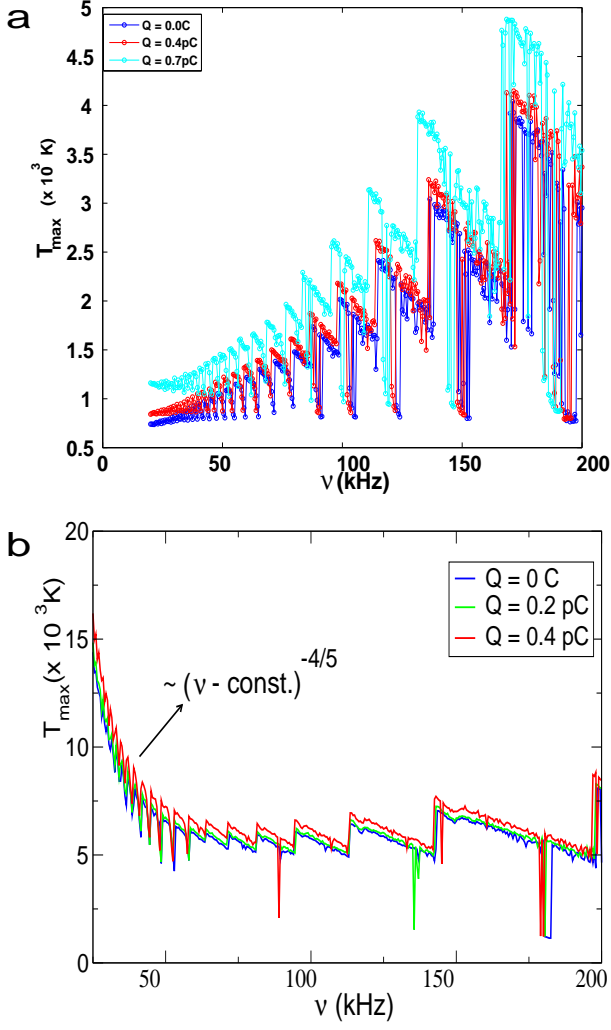


FIG. 13: Maximum temperature T_{max} vs. ν for different values of charge Q at (a) $P_s = 1.1P_0$ (lower / medium pressure, $P_s < P_{tr}$) & (b) $P_s = 1.25P_0$ (high pressure, $P_s > P_{tr}$); the contrasting behavior above and below P_{tr} can be seen. (color online).

reached. As seen in Fig.(5b), increasing the driving frequency shifts the curves to the right, i.e., the same maximal bubble velocity v_{max} that is obtained at some driving frequency ω_1 for a pressure amplitude P_{s1} is reached for a higher frequency $\omega_2 > \omega_1$ only at a higher pressure $P_{s2} > P_{s1}$. Figs.(5b) and (14) where v_{max} vs. P_s , and P_{tr} vs. Q and T_{max} vs. Q plots respectively are shown for $R_0 = 5\mu\text{m}$ and $2\mu\text{m}$ for charged and uncharged bubble at different driving frequencies, illustrate the effect

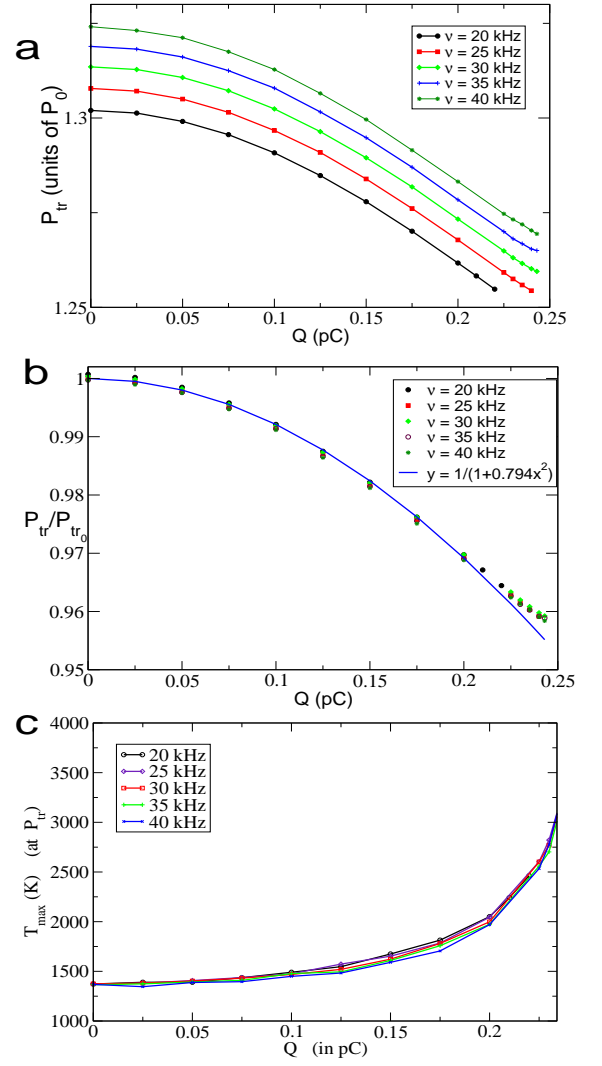


FIG. 14: (a) P_{tr} decreases with increasing Q over all driving frequencies. At a given charge, higher driving frequencies imply higher P_{tr} . (b) The $P_{tr} - Q$ curves when scaled by P_{tr} at $Q = 0$, P_{tr0} , all fall on a master curve obeying eqn.(26). (c) T_{max} vs. Q curves plotted at pressure value equalling the corresponding upper transient threshold value P_{tr} for that particular value of Q , all fall nearly on the same curve. Plots are for $R_0 = 2\mu\text{m}$. (color online).

of driving frequency and charge on bubble velocity, temperature and the location of the upper transient pressure threshold.

The net effect of charge is to raise the possible T_{max} for a bubble in comparison to the uncharged bubble. A comparative plot of T_{max} reached at the upper transient

threshold pressure P_{tr} as a function of charge Q is shown for a few values of the driving frequency ν in Fig.(14).

The temperature T_{max} increases with charge Q for all forcing frequencies.

The value of P_{tr} (for a given bubble-charge, Q) increase with ν . P_{tr} at a given driving frequency decreases with increasing Q . The dependence of P_{tr} on Q over all frequencies can be captured by a normalized plot of P_{tr}/P_{tr0} against Q , where P_{tr0} is the upper transient threshold pressure value at zero charge, for a given frequency. This yields a master curve approximately obeying a relation of the form

$$P_{tr} = \frac{P_{tr0}}{1 + 0.794Q^2}, \quad (26)$$

as seen in Fig.(14b). The maximal value of temperature T_{max} reached in a driven oscillating bubble, at the corresponding, respective P_{tr} (which varies with ν and Q), over all values of charge Q , seems almost independent of the driving frequency ν , as shown in Fig.(14c).

At higher pressures, beyond the upper transient threshold pressure, bubble velocities become larger and of the order of c . We argue that the maximal kinetic energy $\frac{1}{2}M\dot{R}^2 \approx \frac{1}{2}Mc^2$ would approximately equal the dominant electrostatic contribution to the potential energy $Q^2/(4\pi\epsilon R_0)$, so that using $M = 4\pi R_0^3\rho/3$, $Q^2 \sim R_0^4$. This argument is independent of the driving frequency at which the bubble is being forced. At a sufficiently high charge Q_{max} , a bubble of ambient radius R_0 will collapse to the same minimum radius R_{min} , independent of the driving frequency of the forcing pressure amplitude. However, this Q_{max} value will typically be greater than Q_H , the upper bound imposed on the charge Q by the physically realistic requirement that R_{min} does not go below the van der Waals hard-core radius. Thus while this results in Q_H being the greatest, physically realistic value of charge that a bubble can carry, we can still read off the value of a larger $Q = Q_{max}$ from R_{min} vs Q plots at high driving pressures, by identifying the Q at which frequency independence of the curves sets in and all the

curves for different driving frequencies all converge to the same R_{min} . More detailed discussions of R_{min} dependencies are included in our earlier work [23], and we do not show the plots here.

Hence a comparative estimate of this maximal charge a bubble can carry, Q_{max} , for two different values of the initial bubble radius R_0 , say, R_{0a} and R_{0b} , would be obtained from

$$\left(\frac{R_{0a}}{R_{0b}}\right)^2 \sim \left(\frac{Q_{maxa}}{Q_{maxb}}\right), \quad (27)$$

(for larger bubbles, of order $O(\mu\text{m})$ and above). This is essentially a statement that the maximal surface charge density a bubble can carry is approximately same regardless of its initial ambient radius for micrometer and larger bubble radius, given that all other system parameters like the surface tension, pressure conditions, viscosity, etc. remain unchanged, while the influence of the effective surface tension (including the correction for charge present) is predominant in the submicron range. Indeed, for sub-micron and at very small bubble sizes where the surface tension and charge terms become just comparable, we would have instead (comparing electrostatic energy with surface tension or elastic energy) $Q^2/R_0 \sim kR_0^2 = m\omega_b^2 R_0^3$, with $k = m\omega_b^2$ being an effective spring constant and ω_b some natural frequency and m the oscillator mass, so that on substituting for $m = (4/3)\pi\rho R_0^3$, we get

$$\left(\frac{R_{0a}}{R_{0c}}\right)^3 \sim \left(\frac{Q_{maxa}}{Q_{maxc}}\right)^2 \quad (28)$$

for two different values of the initial bubble radius R_0 , R_{0a} and R_{0c} .

That such a non-rigorous approach cannot give any accurate numbers is obvious. Nonetheless, it is useful in giving us rough estimates of the maximal charge that the bubble can carry, in the absence of a constraint such as that imposed by the van der Waals hard-core radius. A comparison of the numbers so obtained in this rough and ready way to that obtained from the numerical results is given below in Table 1 for three different values

of ambient bubble radius R_0 , at $P_s = 1.35P_0$.

TABLE I: Q_{max} ratio from Eqn.(27) (through R_0 ratio) compared with numerical values of Q_{max} from data.

| Table 1 | | | | | |
|------------------|-----------------|-------------|-------------|--|--|
| R_{0a} | R_{0b} | Q_{max_a} | Q_{max_b} | $\left(\frac{R_{0a}}{R_{0b}}\right)^2$ | $\left(\frac{Q_{max_a}}{Q_{max_b}}\right)$ |
| 2 μm | 5 μm | 0.23 pC | 1.24 pC | 0.16 | 0.18 |
| 10 μm | 2 μm | 4.7 pC | 0.23 pC | 25.0 | 20.43 |
| 10 μm | 5 μm | 4.7 pC | 1.24 pC | 4.0 | 3.79 |

VII. CONCLUSIONS

The presence of charge on a bubble suspended in a fluid influences the bubble's oscillations under ultrasonic forcing, and some of the aspects of the dynamics have been addressed in this work, taking the polytropic constant $\Gamma = 5/3$ which governs the equation of state for adiabatic heat transfer. A dimensionless constant ζ which we introduced in an earlier work [23] helps us to identify clearly the Blake threshold and the upper transient threshold P_{tr} for acoustic cavitation. We use this to understand the influence of driving pressure P_s and frequency ν of the applied ultrasonic field on the bubble oscillations. The presence of charge reduces the effective surface tension on the bubble walls so that its maximum radius R_{max} attained during the expansion phase is larger than when it is uncharged; similarly the minimum bubble radius during collapse R_{min} is much smaller in magnitude when the bubble is charged. The charged bubble undergoes a more violent collapse, achieving far higher temperatures in its interior in comparison with the uncharged one. We find that when $P_s < P_{tr}$, the maximum temperatures T_{max} achieved in the bubble increase with increasing ν and charge. For $P_s > P_{tr}$, T_{max} obeys a power law decrease with respect to ν , with an exponent of $-4/5$. The power law behaviour is also obtained analytically through scaling arguments near the regime of Rayleigh collapse.

Bifurcation diagrams of the maximal radial amplitude of the bubble as a function of the driving frequency show the presence of chaotic regimes for $P_s \geq P_{tr}$ for any given ambient bubble radius at fairly large driving frequencies. The route to chaos is through period-doubling followed by period-halving bifurcations. The effect of charge is to always advance these bifurcations. At the lower end of the ultrasound spectral range, for instance in the sonoluminescent regime, the presence of charges do not appear to induce any period-doublings.

Consistent with the fact that the presence of charge has a greater dominating effect over surface tension on bubbles of smaller equilibrium radii [23], the bifurcation diagrams demonstrate that the effect of charges in drastically changing bubble stability is more pronounced for smaller bubbles.

We obtain also the bifurcation diagram of the maximal radial amplitude at any given P_s as a function of the charge at large driving frequency. Here too, period-doublings and period-halvings are seen interspersed with large chaotic regimes.

We obtain analytically an estimate of the minimum charge Q_{min} required on a bubble at a given magnitude of applied pressure to attain a certain value c_1 of the bubble radial velocity. We find that this is related by a simple power law to the driving frequency of the acoustic wave. We show that above a critical frequency ω_H , uncharged bubbles necessarily have to oscillate at velocities below c_1 . The calculations are reproduced numerically also. Further, ω_H depends upon P_s .

Acknowledgments

T.H. acknowledges support through a Rajiv Gandhi National Fellowship from the University Grants Commission, New Delhi.

-
- [1] Lord Rayleigh, “On the pressure developed in a liquid during the collapse of a spherical cavity”, *Philos. Mag.* **34**, 94-98 (1917).
- [2] M. Plesset, “The dynamics of cavitation bubbles”, *J. Appl. Mech.* **16**, 277-282 (1949).
- [3] M. Plesset, “On the stability of fluid flows with spherical symmetry”, *J. Appl. Mech.* **25**, 96-98 (1954).
- [4] E. A. Neppiras, “Acoustic cavitation”, *Phys. Rep.* **61**, 159-251 (1980).
- [5] M. Plesset and A. Prosperetti, “Bubble dynamics and cavitation”, *Ann. Rev. Fluid Mech.* **9**, 145-185 (1977).
- [6] C. E. Brennen, “*Cavitation and Bubble Dynamics*”, Oxford University Press, New York, (1995).
- [7] K. S. Suslick, “Sonochemistry”, *Science* **247**, 1439-1445 (1990).
- [8] M. P. Brenner, S. Hilgenfeldt and D. Lohse, “Single-bubble sonoluminescence”, *Rev. Mod. Phys.* **74**, 425-484 (2002).
- [9] T. Alty, “The cataphoresis of gas bubbles in water”, *Proc. Roy. Soc. (London)* **106**, 315-320 (1924).
- [10] T. Alty, “The origin of the electrical charge on small particles in water”, *Proc. Roy. Soc. (London) A* **112**, 235-251 (1926).
- [11] M. B. Shiran and D. J. Watmough, “An investigation on the net charge on gas bubble induced by 0.75MHz under standing wave condition”, *Iranian Phys. J.* **2**, 19-25 (2008).
- [12] M. B. Shiran, M. Motevalian, R. Ravanfar and S. Bohlooli, “The Effect of Bubble Surface Charge on Phonophoresis: Implication in Transdermal Piroxicam Delivery”, *Iranian J. Pharm. Ther.* **7**, 15-19 (2008).
- [13] J. B. Keller and M. Miksis, “Bubble oscillations of large amplitude”, *J. Acoust. Soc. Am.* **68**, 628-633 (1980).
- [14] J. B. Keller and I. I. Kolodner, “Damping of underwater bubble oscillations”, *J. Appl. Phys.* **27**, 1152-1161 (1956).
- [15] A. I. Grigor’ev and A. N. Zharov, “Stability of the equilibrium states of a charged bubble in a dielectric fluid”, *Technical Physics* **45**, 389-395 (2000).
- [16] H. A. McTaggart, “The electrification at liquid-gas surfaces”, *Phil. Mag.* **27**, 297-314 (1914).
- [17] V. A. Akulichev, “Hydration of ions and the cavitation resistance of water”, *Sov. Phys. Acoust.* **12**, 144-149 (1966).
- [18] Anthony A. Atchley, “The Blake threshold of a cavitation nucleus having a radius-dependent surface tension”, *J. Acoust. Soc. Am.* **85**, 152-157 (1989).
- [19] U. Parlitz, V. Englisch, C. Scheffczyk and W. Lauterborn, “Bifurcation structure of bubble oscillators”, *J. Acoust. Soc. Am.* **88**, 1061-1077 (1990).
- [20] R. Löfstedt, B.P. Barber and S.J. Putterman, “Towards a hydrodynamic theory of sonoluminescence”, *Phys. Fluids A* **5**, 2911-2928 (1993).
- [21] Z.C. Feng and L.G. Leal, “Nonlinear bubble dynamics”, *Ann. Rev. Fluid Mech.* **29**, 201-243 (1997).
- [22] S. Hilgenfeldt, M. P. Brenner, S. Grossmann and D. Lohse, “Analysis of Rayleigh-Plesset dynamics for sonoluminescing bubbles”, *J. Fluid Mech.* **365**, 171-204 (1998).
- [23] T. Hongray, B. Ashok and J. Balakrishnan, “Effect of charge on the dynamics of an acoustically forced bubble”, submitted, (2013).
- [24] W. Lauterborn and E. Suchla, “Bifurcation superstructure in a model of acoustic turbulence”, *Phys. Rev. Lett.* **53**, 2304-2307 (1984).
- [25] P. Smereka, B. Birnir and S. Banerjee, “Regular and chaotic bubble oscillations in periodically driven pressure fields”, *Phys. Fluids* **30**, 3342-3350 (1987).
- [26] W. Lauterborn and U. Parlitz, “Methods of chaos physics and their applications to acoustics”, *J. Acoust. Soc. Am.* **84**, 1975-1993 (1988).
- [27] R.G. Holt, D.F. Gaitan, A.A. Atchley and J. Holzfuss, “Chaotic Sonoluminescence”, *Phys. Rev. Lett.* **72**, 1376-1379 (1994).
- [28] C. C. Wu and P. H. Roberts, “a model of sonoluminescence”, *Proc. R. Soc. London A* **445**, 323-349 (1994).
- [29] K. Yasui, “Alternative model of single-bubble sonoluminescence”, *Phys. Rev. E* **56**, 6750-6760 (1997).